Measurement of ρ^o and ϕ-Meson Electroproduction*

J. T. Dakin, G. J. Feldman, W. L. Lakin,†
F. Martin, M. L. Perl, E. W. Petraske,‡ and W. T. Toner§
Stanford Linear Accelerator Center, Stanford University, Stanford, California 94305
(Received 22 March 1973)

We report measurements of ρ^0 and ϕ electroproduction at 19.5 GeV in a wide-aperture spectrometer which detected the scattered electron and the decay products of the vector mesons. Data are presented for the region of virtual-photon mass squared $q^2 = -0.25$ to -2.0 $(\text{GeV}/c)^2$ and virtual-photoproduction center-of-mass energy squared $s = 10$ to 30 GeV^2. As $|q^2|$ increases, the ρ mass spectrum shape changes and the momentum-transfer distribution broadens. The ratio of the ρ cross section to the total cross section decreases from 11% at $q^2 = 0$ to about 6% at $|q^2| = m_\rho{}^2$. The ratio for the production of longitudinally to transversely polarized ρ^0 mesons is $0.45^{+0.15}_{-0.10}$ at $|q^2| = m_\rho{}^2$, and the interference between longitudinal and transverse amplitudes is almost maximal. The relative ϕ-meson cross section also decreases as $|q^2|$ increases. Unitary lower bounds on the longitudinal-transverse ratio in inelastic electron scattering are derived.

I. INTRODUCTION

Many photoproduction processes can be understood by assuming that the photon couples directly to vector-meson states. By studying vector-meson electroproduction we seek to determine how this coupling evolves as the photon becomes space-like and its polarization has longitudinal as well as transverse components.

We report here measurements of ρ^0 and ϕ meson electroproduction which combine high virtual photon energies and the ability to study ρ^0 production and decay angular correlations. These measurements were made at the Stanford Linear Accelerator Center (SLAC) using a wide-aperture spark chamber spectrometer. This paper is a more complete account of data reported earlier.[1]

The first attempts to measure ρ^0 electroproduction used a missing (ρ^0) mass technique in which the scattered electron and recoil proton were detected in coincidence.[2-3] These experiments suffered from a large background, which made the

extraction of the vector-meson signal difficult. Furthermore, the ρ^0 polarization could not be measured in such experiments since the decay pions were not detected. A spectrometer experiment at DESY detected the scattered electron and the pions from the ρ^0 decay, but at angles such that only transversely polarized ρ^0 mesons could be observed.[4] In addition to the experiment reported here, two other experiments have been performed in which the decay pions can be observed over a wide range of angles. One was performed using a streamer chamber at DESY[5] and the other was performed with a hybrid bubble chamber at SLAC.[6] Both experiments were conducted at lower virtual-photoproduction center-of-mass energies than the present experiment. No previous experiments have observed ϕ-meson electroproduction.

The electroproduction of vector mesons has been studied theoretically in vector-meson-dominance (VMD) models[7-8] and by several other approaches.[9] In a recent series of papers, Sakurai and

Schildknecht have attempted to understand inelas-
tic electron-nucleon scattering in terms of vir-
tual-photon couplings to vector-meson states.[10]
Their work makes a number of testable predic-
tions for vector-meson electroproduction, includ-
ing the prediction that the ratio of longitudinal to
transverse ρ^0 production is quite small, about
0.06 at $|q^2| = m_\rho^2$.

For the most part this paper will deal with ρ^0
production, with ϕ-meson production relegated to
Sec. VI. Kinematics and phenomenology will be
discussed in Sec. II. Section III will describe the
apparatus and Sec. IV will describe the data collec-
tion and reduction. The results for ρ^0 production
will be given in Sec. V. Section VII will derive
lower bounds to the ratio of longitudinal to trans-
verse total virtual-photoproduction cross sections
using unitarity and the Schwarz inequality.

II. KINEMATICS AND PHENOMENOLOGY

The ρ electroproduction reaction

$$ep \rightarrow ep\pi^+\pi^- \tag{1}$$

can be regarded as an inelastic electron scattering
$(e \rightarrow e\gamma^*)$, followed by the virtual photoproduction
of a ρ $(\gamma^* p \rightarrow \rho p)$, followed by the ρ decay $(\rho \rightarrow \pi^+\pi^-)$.
Quantities describing the electron scattering are
q^2, the square of the four-momentum carried by
the photon; ϵ, the photon polarization; and s, the
square of the total energy in the $\gamma^* p$ collision as
measured in the $\gamma^* p$ center-of-mass system. The
ρ production is characterized by t', the four-
momentum transfer squared to the proton less its
smallest possible value (t_{min}), and by ϕ_e, the
azimuthal angle between the electron scattering
plane and the ρ production plane. θ^* is the angle
between the γ^* and the ρ in the $\gamma^* p$ center-of-
mass system. The final $\pi^+\pi^-$ system is described
by $m_{\pi\pi}$, its invariant mass; ϕ, the azimuthal angle
between the ρ production plane and the ρ decay
plane; and θ, the ρ decay polar angle. The def-
inition of the various angles is shown in Fig. 1.
It proved useful in the analysis to define an ad-
ditional angle $\psi \equiv \phi_e + \phi$. In the limit $\theta^* \rightarrow 0$, ψ be-
comes the azimuthal angle between the electron
scattering plane and the ρ decay plane.

The electron-scattering variables can be ex-
pressed as follows:

$$q^2 = -4EE'\sin^2(\tfrac{1}{2}\theta_e), \tag{2}$$

$$s = m^2 + 2m\nu + q^2, \tag{3}$$

$$\epsilon = \left[1 + 2\left(1 - \frac{\nu^2}{q^2}\right)\tan^2(\tfrac{1}{2}\theta_e)\right]^{-1}, \tag{4}$$

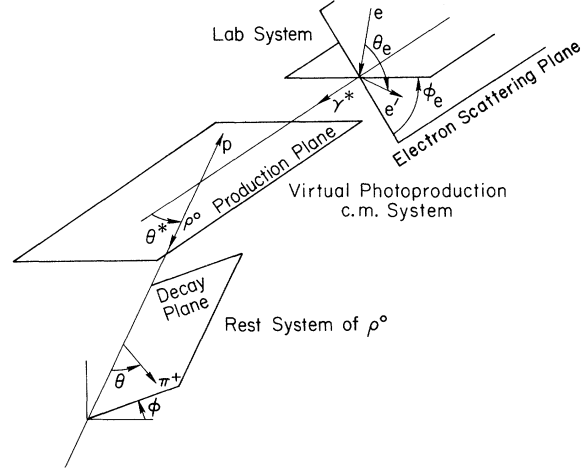where E and E' are the initial and scattered elec-

FIG. 1. Coordinate systems and angles for ρ^0 electro-
production.

tron energies in the laboratory system, m is the
mass of the target proton, $\nu = E - E'$, and the elec-
tron mass is neglected. In our metric $q^2 \leq 0$.

The polarization of the virtual photon can be
given as the incoherent sum of two pure states,
$\vec{\epsilon}_a$ and $\vec{\epsilon}_b$:

$$\vec{\epsilon}_a = \{[\tfrac{1}{2}(1+\epsilon)]^{1/2}, 0, -\epsilon_L^{1/2}\}, \tag{5a}$$

$$\vec{\epsilon}_b = \{0, [\tfrac{1}{2}(1-\epsilon)]^{1/2}, 0\}, \tag{5b}$$

where the polarization vector components are
transverse in the electron scattering plane, trans-
verse out of the electron scattering plane, and
longitudinal, respectively.[11] The parameter ϵ_L
is defined as

$$\epsilon_L = \frac{-q^2}{q_0^2}\epsilon. \tag{6}$$

We follow the usual practice of absorbing the
frame-dependent factor $(-q^2/q_0^2)$ into the produc-
tion cross section and replacing ϵ_L by ϵ. Equa-
tion (5a) shows that longitudinally polarized virtual
photons will be coherent with virtual photons po-
larized in the electron scattering plane, allowing
the possibility of observing transverse-longitudi-
nal interference effects.

This experiment measures the ratio of the vir-
tual-photoproduction cross section for vector-
meson production to the total virtual-photoproduc-
tion cross section directly. To obtain virtual-
photoproduction cross sections in absolute units,
it is necessary to specify a convention for the flux
of virtual photons. We use the usual Hand con-
vention[12] to relate the electron scattering cross
section $d\sigma/dq^2 ds$ to the total virtual-photoproduc-
tion cross section $\sigma_{tot}(q^2, s)$:

SPARK
CHAMBERS

FLUX RETURN

MAGNETIC
FIELD

TARGET

BEAM

SUPERCONDUCTING
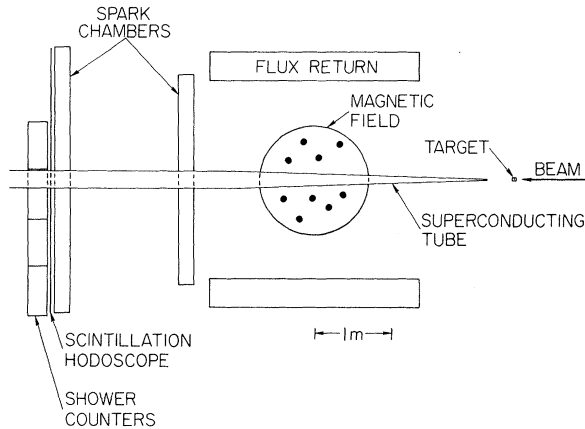TUBE

SCINTILLATION
HODOSCOPE

SHOWER
COUNTERS

⊢—1m—⊣

FIG. 2. Schematic elevation view of the apparatus.

$$\frac{d\sigma}{dq^2 ds} = \Gamma \sigma_{\text{tot}}(q^2, s), \tag{7}$$

where

$$\Gamma = \frac{\alpha}{8\pi} \frac{s - m^2}{m^2 E^2 (-q^2)(1 - \epsilon)} \quad . \tag{8}$$

III. APPARATUS

The experimental apparatus consisted of a 19.5-GeV electron beam incident on a 4-cm liquid hydrogen target and a large-aperture spectrometer to detect a large fraction of the forward final-state particles with lab momenta greater than ~1 GeV/c. These elements are shown in Fig. 2 and discussed in greater detail below.

The electron beam contained typically 10^4 e^- per 1.5-μsec-long SLAC pulse. At the experimental target, the beam had an rms width of 0.5 mm×0.5 mm and an rms divergence less than 0.2 mrad ×0.2 mrad. There the beam was very well collimated, with fewer than one in 10^5 e^- outside a 0.5-cm-diameter circle. The momentum spread in the beam was 0.2%.

The spectrometer magnet has 1.37-m-diameter pole faces separated by 0.91 m. It was centered on the beam line, 2.54 m downstream from the target, with its principal field component horizontal. At the magnet center, this field was 10 kG and the field integral was 17 kG m.

The unscattered beam and the forward electromagnetic backgrounds passed through the magnet in a field-free region created by a cylindrical superconducting tube.[13] Beyond the magnet were two optical spark chambers separated by 1.7 m. The chambers had inactive holes through their centers, where the beam tube passed. The apertures of the magnet, spark chambers, and beam tube produced the acceptance shown in Fig. 3.
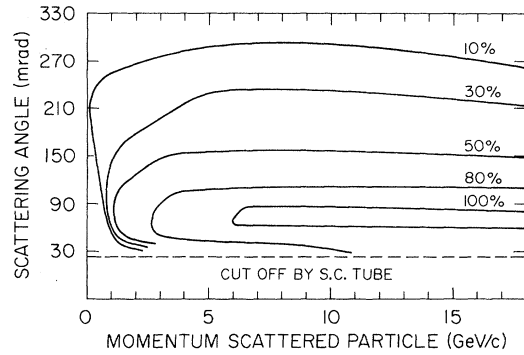

FIG. 3. Geometric acceptance of the apparatus averaged over the azimuthal angle.

The apparatus was triggered on the detection of a scattered electron by a hodoscope of 20 scintillation counters and 11 shower counters[14] behind the second spark chamber. The shower-counter thresholds were set to ~4 GeV. Photon triggers were eliminated by the requirement that a shower counter fire coincident with the scintillators in front of it. The kinematic range of inelastic electron scatters covered by this trigger was roughly $|q^2| > 0.3$ (GeV/$c)^2$, $\nu < 15$ GeV. There was no hadron requirement in the trigger.

For each trigger a single picture was taken of the optical spark chambers on 70-mm film. The camera was located in the horizontal plane 21.6 m from the beam line with its optic axis aligned perpendicular to the beam. Each picture contained four views of each chamber: a direct view, a top and a bottom view in small-angle stereo, and a rear view to expose tracks blocked in the direct view by a beam pipe. Figure 4 contains a picture of an event which is a candidate for an elastically produced ρ meson.
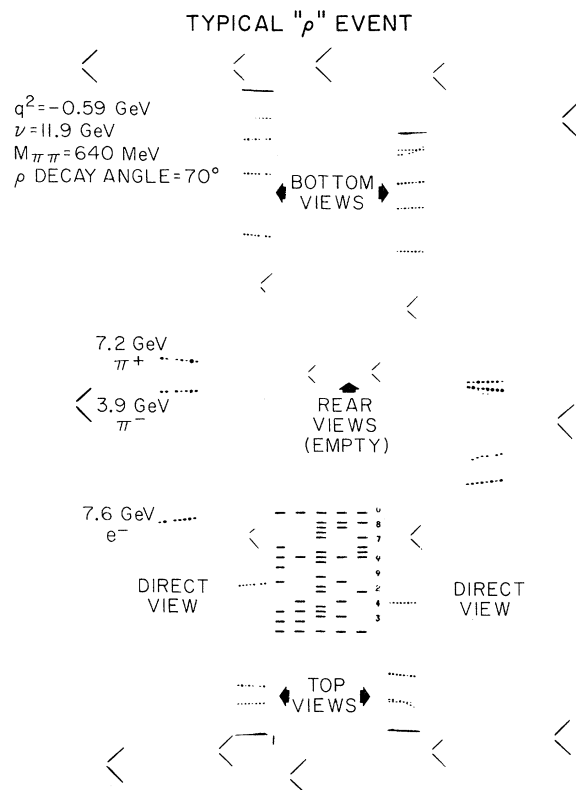
A PDP-8 computer recorded scintillation and shower-counter status, shower-counter pulse heights, and scintillation-counter timing information for each event.

The beam flux was integrated by a quantameter located behind the shower counters and was monitored instantaneously by a surface-barrier detector.[15]

IV. DATA COLLECTION AND REDUCTION

We recorded 250 000 pictures with the H_2 target corresponding to 2.6×10^{12} incident electrons. All of the film was measured by a flying-spot digitizer, Hummingbird II,[16] and selected samples were also measured by a conventional manual system.

The momentum of each reconstructed track was computed by propagating the track back through the magnet and adjusting the momentum until the

TYPICAL "ρ" EVENT

$q^2 = -0.59$ GeV
$\nu = 11.9$ GeV
$M_{\pi\pi} = 640$ MeV
ρ DECAY ANGLE = 70°

BOTTOM VIEWS

7.2 GeV
π^+

3.9 GeV
π^-

REAR VIEWS (EMPTY)

7.6 GeV
e^-

DIRECT VIEW   DIRECT VIEW

TOP VIEWS

FIG. 4. Photograph of a typical ρ-like event.

$\gamma^* p \longrightarrow \pi^+ \pi^- X$

FIG. 5. Missing mass squared for events with dipion mass in the range 0.6 to 0.9 GeV.

track intercepted the target vertically. Tracks which did not, then, strike the target horizontally were rejected. The rms momentum resolution was 2% at 10 GeV.

In each reconstructed picture, the electron was identified by matching the positions and momenta of tracks to the position and pulse height of the shower counter which triggered the event. Remaining tracks which were consistent with the scintillator hodoscope pattern were assumed to be hadrons.

The number of electrons in each q^2-s interval was corrected for geometric efficiency, measuring losses, hadron contamination (0–7%), and radiative effects (10–48%).[17] The result was the total number of virtual-photon interactions in the data in that q^2-s interval, or effectively the $\gamma^* p$ total cross section $\sigma_{tot}(q^2, s)$.

Each event with three or more tracks was measured three times by the manual system to see whether it contained an e, π^+, π^- combination consistent with reaction (1). The missing mass squared of events with an electron and two hadrons with dipion mass in the ρ region is shown in Fig. 5. There is a large peak at the mass squared of a proton. The width of the peak is consistent with
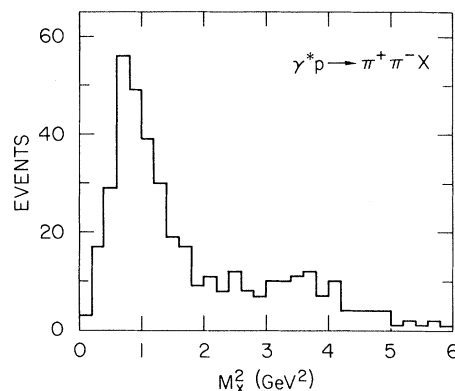
the experimental resolution and the tail at high missing mass is due to radiation and inelastic production of ρ^0 mesons. Cuts in missing mass squared were made at 0.2 and 1.6 GeV^2 and a 1-c fit was made to the events in this interval. There were 238 "ρ" events surviving this process in the kinematic range $-0.25 > q^2 > -2.00$ (GeV/c)^2, $10 < s < 30$ GeV^2, $0 > t' > -0.7$ (GeV/c)^2, and 0.6 $< m_{\pi\pi} < 0.9$ GeV. These events were divided into three q^2 bins whose average properties are given in Table I.

The events in each bin were fitted by a maximum-likelihood technique to the form

$$\frac{d\sigma_\rho(q^2, s)}{dt' d\phi_e d\psi d\cos\theta} = \sigma_{tot}(q^2, s) \frac{\sigma_\rho}{\sigma_{tot}} b e^{bt'} W(\phi_e, \psi, \theta) .$$

(9)

The fitting function contained the normalization $\sigma_{tot}(q^2, s)$ determined by counting electrons and the detailed dependence of the geometric efficiency on the independent variables q^2, s, t, ϕ_e, ψ, and $\cos\theta$. The output from the fit included the ratio of the virtual-photoproduction cross section for ρ production to the total virtual-photoproduction cross section, σ_ρ/σ_{tot}; the slope parameter b; and parameters from the angular correlation term W to be described later.

The normalized cross section, σ_ρ/σ_{tot}, was corrected for elastic ρ losses due to radiation,[18] the missing mass cut, the $m_{\pi\pi}$ cut, scanning and measuring losses, and numerous small instrumental effects. A correction was also made for the number of $\pi\pi$ events in the $m_{\pi\pi}$ interval used which were not elastic ρ events. These corrections are tabulated in Table II along with an estimate of the uncertainty in each. The over-all systematic uncertainty in σ_ρ/σ_{tot} is estimated to be 16%. The error bars indicated in the figures represent statistical errors only.

TABLE I. Average properties of the three bins in q^2.

	$-0.25 > q^2 > -0.5$	$-0.5 > q^2 > -1.0$	$-1.0 > q^2 > -2.0$	$(\text{GeV}/c)^2$
$\langle q^2 \rangle$	-0.36	-0.70	-1.27	$(\text{GeV}/c)^2$
$\langle s \rangle$	22.6	19.6	19.8	GeV^2
$\langle \epsilon \rangle$	0.67	0.74	0.72	
$\langle \nu \rangle$	11.7	10.4	10.7	GeV
$\langle \omega \rangle$ [a]	63.4	29.2	16.5	
$\langle t_{\min} \rangle$	-0.008	-0.015	-0.033	$(\text{GeV}/c)^2$

[a] $\omega \equiv -2m\nu/q^2$.

V. RESULTS FOR ρ^0 ELECTROPRODUCTION

A. Mass Spectra

Figure 6 shows the invariant mass distribution of all pion pairs consistent with the hypothesis of reaction (1). The dipion mass spectrum is dominated by the ρ^0 meson with little or no background. Some of the events with dipion mass less than 0.4 GeV are consistent with the hypothesis

$$\gamma^* p \to \phi p$$
$$\searrow K^+ K^- . \tag{10}$$

These events will be discussed in Sec. VI.

In experiments conducted at lower center-of-mass energies, there is some difficulty in separating the ρp and $\pi \Delta$ final states.[5] This source of background is not present in this experiment because (1) the $\pi \Delta$ cross section falls as s^{-2} while the ρp cross section is relatively constant in s,[19] (2) the overlap region in the Dalitz plot between the ρp and $\pi \Delta$ final states decreases with increas-

TABLE II. Correction factors applied to $\sigma_\rho/\sigma_{\text{tot}}$. The numbers in parentheses indicate the percentage uncertainty in the indicated factor. The corrections were substantially the same for each of the q^2 bins. The 16% over-all systematic uncertainty includes additional contributions from the electron detection efficiency, the radiative corrections to σ_{tot}, and knowledge of the acceptance.

Missing-mass cuts	1.09 (4)
Radiative effects	1.24 (5)
Scanning losses	1.05 (5)
Measuring losses	1.05 (5)
Counter positions and dead time	1.04 (2)
Pion decay in flight	1.02 (0)
Pion absorption	1.01 (0)
Ambiguous events	1.04 (0)
Background	0.95 (5)
Dipion-mass cuts	1.29 (7)
Total	2.04 (16)

ing s, and (3) the experimental acceptance for this region of the Dalitz plot is small. This is shown in Fig. 7, where the $\pi^+ p$ invariant mass has been plotted for the "ρ" events. There are no events at the mass of the Δ^{++}.

To study possible changes in the ρ^0 mass spectrum as a function of q^2, we fitted the data in the range $0.44 < m_{\pi\pi} < 1.04$ GeV in each q^2 bin to the form

$$\frac{d\sigma}{dm_{\pi\pi}} = \left(\frac{m_\rho^2}{m_{\pi\pi}^2} \right)^{n/2} B(m_{\pi\pi}), \tag{11}$$

where $B(m_{\pi\pi})$ is relativistic p-wave Breit-Wigner shape[20]:

$$B(m_{\pi\pi}) = \frac{2}{\pi} \frac{m_\rho m_{\pi\pi} \Gamma(m_{\pi\pi})}{(m_\rho^2 - m_{\pi\pi}^2)^2 + m_\rho^2 \Gamma^2(m_{\pi\pi})}, \tag{12}$$

where

$$\Gamma(m_{\pi\pi}) = \Gamma_0 \left(\frac{q_{\pi\pi}}{q_\rho} \right)^3 \frac{m_\rho}{m_{\pi\pi}} \tag{13}$$
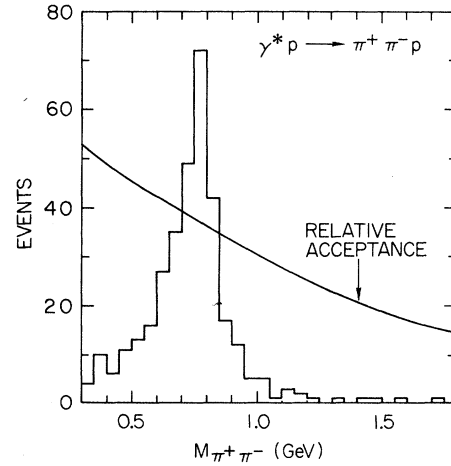

FIG. 6. Dipion mass spectrum for all events in which the missing mass is consistent with that of a proton. The curve represents the relative acceptance averaged over all other variables.
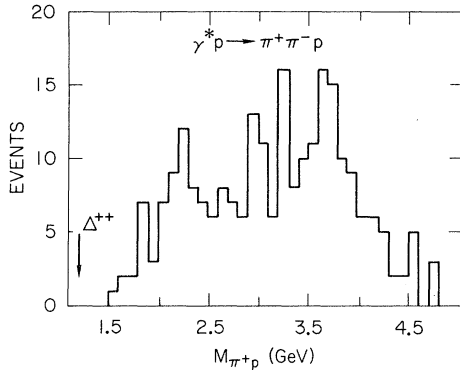
FIG. 7. Invariant $\pi^{+}p$ mass for events which are consistent with the hypothesis of ρ^{0} electroproduction.

and

$$q = \tfrac{1}{2}(m^{2} - 4m_{\pi}^{2})^{1/2} \, . \tag{14}$$

The mass ($m_{\rho} = 0.77$ GeV) and width ($\Gamma_{0} = 0.145$ GeV) were fixed at photoproduction values.[21] The photoproduction data were fitted in an identical manner. All of the data were fitted well by Eq. (11). When a flat background term was added to Eq. (11), the fitted values of n did not change appreciably and backgrounds selected by the fits were between 0 and 5%. The fitted values of n are shown in Fig. 8. The ρ mass shape appears to become more "normal" as $|q^{2}|$ increases. This effect was predicted by a diffraction-dissociation model,[22] but the prescription given by that model,

$$\left(\frac{m_{\rho}^{2}}{m_{\pi\pi}^{2}}\right)^{n/2} \rightarrow \left(\frac{m_{\rho}^{2} - q^{2}}{m_{\pi\pi}^{2} - q^{2}}\right)^{n/2} \, , \tag{15}$$

provides a more drastic change in the ρ mass spectrum for $|q^{2}| \lesssim m_{\rho}^{2}$ than is indicated by the data.

B. Momentum Transfer Distributions

We fitted the t' distribution to the form $e^{bt'}$ in the range $0 > t' > -0.7$ $(\text{GeV}/c)^{2}$ in each of the q^{2} bins. All of the data were fitted well by this form. The results of these fits are shown in Fig. 9 along with photoproduction results,[21,23] which have been analyzed in the same manner as our data. The b parameter appears to decrease with increasing $|q^{2}|$.

The DESY streamer-chamber[5] and SLAC hybrid-bubble-chamber[6] experiments also indicate a decrease in the b parameter with increasing $|q^{2}|$. Reported values of the b parameter from these experiments are generally lower than those from this experiment, and this is presumably accounted for by the difference in average center-of-mass energies. To try to remove the variation in s, in Fig. 10 we have plotted the ratio of the electroproduction b parameters to the photoproduction
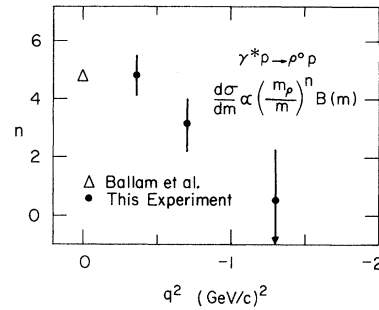

FIG. 8. The parameter n defined in Eq. (11). Photoproduction data ($q^{2} = 0$) are taken from Ref. 21.

values at the same value of s. When viewed in this way, the results of all three experiments are in reasonable agreement.

Another approach to understanding the momentum transfer distributions as a function of q^{2} and s has been proposed by Nieh.[24] He presents a physical picture in which the effective size of the photon is related to the amount of time, Δt, that an associated hadronic system can exist. Δt is calculated using the uncertainty principle. In electroproduction of ρ^{0} mesons,

$$\Delta t \approx \frac{2\nu}{m_{\rho}^{2} - q^{2}} \tag{16}$$

and the b parameter should be a function of Δt only. The data are in qualitative agreement with this approach.

We have also determined the t' distribution separately for longitudinally and transversely polarized ρ^{0} mesons and have found no significant difference between them.

C. Angular Distributions

The decay distribution of the ρ meson serves as an analyzer of its polarization. Thus the correla-
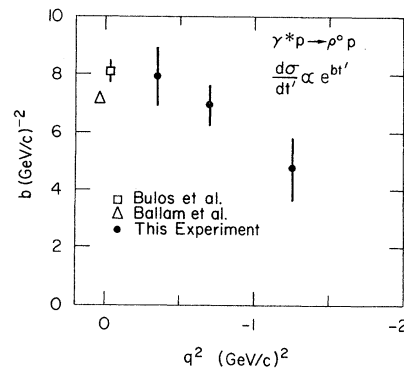

FIG. 9. The b parameter from fits to the form $e^{bt'}$. Photoproduction data ($q^{2} = 0$) are taken from Refs. 21 and 23.

tions between the production and decay angles can yield information on the production mechanism. The complete angular distributions have been given by Dieterle.[25] In his notation,

$$W(\phi_e, \theta, \phi) = \sum_{\substack{\lambda\lambda' \\ \sigma\sigma'}} B^{\lambda\lambda'}(\epsilon, \phi_e) \rho_{\sigma\sigma'}^{\lambda\lambda'} A_{\sigma\sigma'}(\theta, \phi), \quad (17)$$

where $B^{\lambda\lambda'}$ is the photon density matrix, $A_{\sigma\sigma'}$ is the ρ decay matrix, $\rho_{\sigma\sigma'}^{\lambda\lambda'}$ is the production matrix, and the summation is taken over the photon helicities (λ, λ') and the ρ helicities (σ, σ'). $B^{\lambda\lambda'}$ and $A_{\sigma\sigma'}$ are known functions, and $\rho_{\sigma\sigma'}^{\lambda\lambda'}$ is, in principle, to be determined from experiment. The production matrix has 81 elements, but parity conservation and Hermiticity reduce the number of independent elements to 25.

We have studied the angular correlations in the data for evidence of nonhelicity-conserving amplitudes (production matrix elements for which $\lambda \neq \sigma$ or $\lambda' \neq \sigma'$) and have failed to find any at the 10% level, the statistical level of this experiment. Thus we have assumed that s-channel helicity conservation holds in electroproduction, as it does in photoproduction.[21] In this case Eq. (17) reduces to

FIG. 10. The ratio of electroproduction to photoproduction b parameters (from fits to the form $e^{bt'}$ or e^{bt}) at the same value of s. Data from this experiment and Refs. 5 and 6 are shown.

$$W(\theta, \psi) = \frac{3}{8\pi^2(1 + \epsilon R_\rho)} \{\epsilon R_\rho \cos^2\theta + \tfrac{1}{2} \sin^2\theta (1 + \epsilon \cos 2\psi) - [\epsilon R_\rho (1 + \epsilon)/2]^{1/2} \cos\delta \sin 2\theta \cos\psi\}, \quad (18)$$

where R_ρ is the ratio for the production of longitudinally to transversely polarized ρ^0 mesons and δ is the phase angle between the longitudinal and transverse amplitudes. The results of the fits for R_ρ and $\cos\delta$ are given in Figs. 11(a) and 11(b).

We have fitted R_ρ to the form suggested by the VMD model of Sakurai and Schildknecht,[10]

$$R_\rho = -\xi^2 \frac{q^2}{m_\rho^2}. \quad (19)$$

The data are adequately described by this fit with $\xi^2 = 0.45^{+0.15}_{-0.10}$. However, this value of ξ^2 is not consistent with the value required by their model to fit inelastic electron scattering results, $\xi^2 \approx 0.06$.

Eckardt *et al.*[5] report a value of $R_\rho = 0.30 \pm 0.14$ at $\langle q^2 \rangle = -0.6$ $(\text{GeV}/c)^2$ and $\langle s \rangle = 5.3$ GeV². Preliminary results for R_ρ from the SLAC hybrid-bubble-chamber experiment are in excellent agreement with our measurements.[26]

The measurements of $\cos\delta$ plotted in Fig. 11(b) show almost maximal interference between transverse and longitudinal amplitudes. This interference term is evidenced by the clustering of events in the $\cos\theta$-ψ scatter plot (Fig. 12). Both raw data and data approximately corrected for the geometrical acceptance are shown.

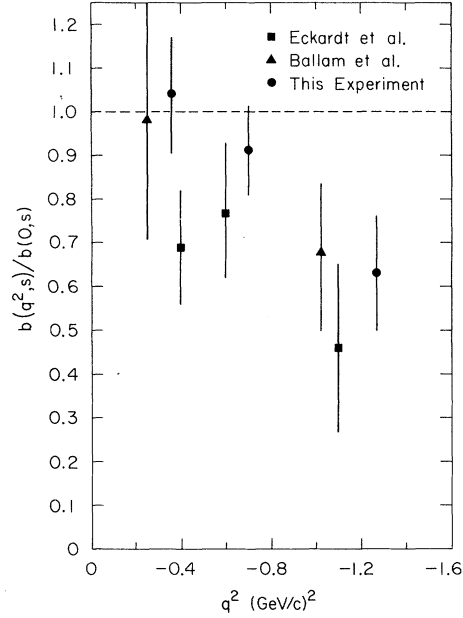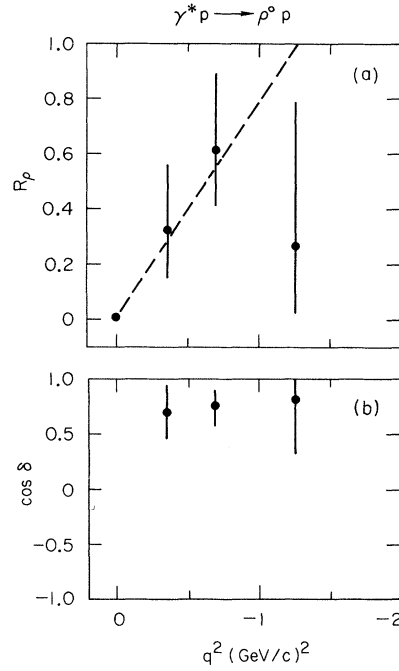For a purely diffractive production process $\cos\delta$

FIG. 11. (a) The ratio of longitudinal to transverse ρ^0 production. The dashed line is the best fit to Eq. (19). (b) Cosine of the longitudinal-transverse phase difference.

should be unity. Again the preliminary results of the SLAC hybrid-bubble-chamber experiment for $\cos\delta$ are in excellent agreement with our measurements,[26] but the DESY streamer-chamber experiment reports no evidence for transverse-longitudinal interference.[5]

D. Total ρ^0 Cross Sections

Figure 13 shows the ratio of the ρ^0 virtual-photoproduction cross section to the total virtual-photoproduction cross section. Photoproduction cross section ratios, which were obtained by similar analysis methods, are also shown. The ρ^0 cross section drops faster than the total virtual-photoproduction cross section and also faster than the prediction of the VMD model,[10]
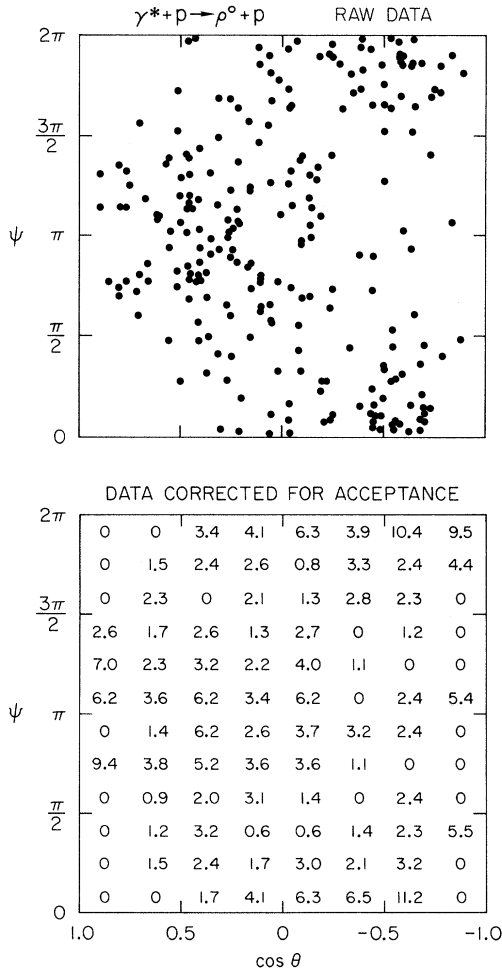
FIG. 12. Scatter plots of the data as a function of ψ and $\cos\theta$. The top plot is of the raw data and the bottom plot is of data approximately corrected for geometrical acceptance.
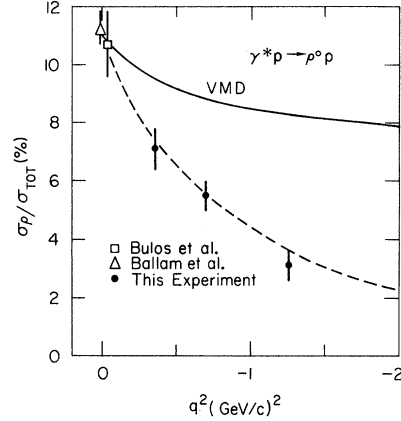
FIG. 13. The ratio of the ρ^0 virtual-photoproduction cross section to the total virtual-photoproduction cross section. The solid curve represents the prediction of the VMD model, Eq. (20), and the dashed curve represents Eq. (21). Photoproduction data $(q^2 = 0)$ are taken from Refs. 21 and 23.

$$\frac{d\sigma_\rho(q^2)}{dt}\bigg|_{t=0} = \frac{d\sigma_\rho(0)}{dt}\bigg|_{t=0} \frac{(1 - \epsilon\,\xi^2 q^2/m_\rho^2)}{(1 - q^2/m_\rho^2)^2}, \qquad (20)$$

with $\xi^2 = 0.45$. We note, however, that the data can be described by the simple form

$$\sigma_\rho(q^2) = \sigma_\rho(0)\,\frac{e^{bt_{min}}}{(1 - q^2/m_\rho^2)^2}. \qquad (21)$$

Both Eqs. (20) and (21) are displayed in Fig. 13 in terms of cross-section ratios. The $e^{bt_{min}}$ factor in Eq. (21) is relatively unimportant, contributing only 15% for the highest $|q^2|$ bin.

There is general experimental agreement that the ρ^0 virtual-photoproduction cross section falls substantially faster than the total virtual-photoproduction cross section as $|q^2|$ increases.[4-6]

All of our results for ρ^0 production are summarized in Table III.

VI. ϕ ELECTROPRODUCTION

The data reduction procedure was repeated for electron and two hadron combinations with the assumption that the hadrons were K mesons. Figure 14 shows the dikaon mass distribution for events consistent with the hypothesis

$$\gamma^* p \rightarrow K^+ K^- p . \qquad (22)$$

There are six events at the mass of the ϕ meson. We estimate that the background from electron, muon, and pion pairs is 1 ± 1 event. The average q^2 of the events is -0.6 $(\text{GeV}/c)^2$ and the average s is 22.9 GeV^2. The acceptance for ϕ's was 60% larger than that for ρ^0's; the corrections were similar except for meson mass cut, K decay, and

TABLE III. ρ^0 electroproduction results. The errors are statistical only.

		$\langle q^2 \rangle$	-0.36	-0.70	-1.27	$(\text{GeV}/c)^2$
n	[Eq. (11)]		4.8 ± 0.7	3.5 ± 0.9	1.0 ± 1.7	
b	[Eq. (9)]		7.9 ± 1.0	6.9 ± 0.7	4.8 ± 1.0	$(\text{GeV}/c)^2$
R_ρ	[Eq. (18)]		$0.32^{+0.24}_{-0.18}$	$0.63^{+0.28}_{-0.21}$	$0.27^{+0.52}_{-0.25}$	
$\cos\delta$	[Eq. (18)]		$0.70^{+0.24}_{-0.26}$	$0.75^{+0.15}_{-0.17}$	$0.80^{+0.20}_{-0.48}$	
$\sigma_\rho/\sigma_{\text{tot}}$	[Eq. (9)]		0.071 ± 0.007	0.055 ± 0.005	0.031 ± 0.005	
σ_ρ	[Eqs. (7), (9)]		4.6 ± 0.5	2.5 ± 0.2	0.94 ± 0.15	μb

unseen decay modes. These corrections are tabulated in Table IV.

The ratio of the ϕ virtual-photoproduction cross section to the total virtual-photoproduction cross section is 0.0017 ± 0.0009, compared to 0.0046 ± 0.0006 for photoproduction.[21]

VII. UNITARITY LOWER BOUND ON THE LONGITUDINAL-TO-TRANSVERSE RATIO FOR THE TOTAL VIRTUAL-PHOTOPRODUCTION CROSS SECTION

With only a few very reasonable assumptions, we can derive a nontrivial lower bound on the longitudinal-to-transverse ratio for the total virtual-photoproduction cross section from our measurements of ρ^0 electroproduction. We will refer to this ratio as R_{tot} to distinguish it from R_ρ, the longitudinal-to-transverse ratio for ρ^0 electroproduction. At higher values of $|q^2|$, R_{tot} has been determined by single-arm electron-scattering experiments[27] and is conventionally given by

$$R_{\text{tot}} = \left(1 - \frac{\nu^2}{q^2}\right)\frac{W_2}{W_1} - 1 \tag{23}$$

in terms of the usual structure functions.
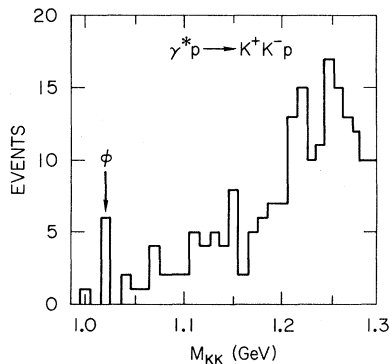
The formalism, an "optical theorem for quasi-

FIG. 14. Dikaon spectrum for events in which the missing mass is consistent with that of a proton when all observed hadrons are assumed to be kaons.

elastic scattering," was first given by Knies, who applied it to predict a lower bound on the total (real) photoproduction cross section based on measurements of ρ^0 photoproduction.[28] Recently Sakurai has applied it to electroproduction[29] using some preliminary data. The only theoretical inputs are the unitarity relation and the Schwarz inequality. No assumption of VMD is needed.

Given any two-body inelastic reaction $a \to b$, from Eq. (5.3) of Ref. 28

$$h(a,b)\frac{d\sigma'}{dt}(a \to b)\bigg|_{\theta=0} \leq \frac{1}{16\pi}\sigma_{\text{tot}}(a)\sigma_{\text{tot}}(b), \tag{24}$$

where $d\sigma'/dt$ indicates the part of the cross section which comes from the imaginary part of the scattering amplitude, and $h(a,b)$ is a kinematical factor required by the reciprocity relation. We rewrite Eq. (24) for the case in which $a = \gamma^*p$ and $b = \rho^0 p$, both in the longitudinal helicity state

$$\sigma_L(\gamma^*p) \geq \frac{16\pi}{\sigma_L(\rho^0 p)}h\frac{d\sigma'}{dt}(\gamma^*p \to \rho^0 p)_L\bigg|_{t=t_{\min}}, \tag{25}$$

where

TABLE IV. Correction factors applied to $\sigma_\phi/\sigma_{\text{tot}}$. The numbers in parentheses indicate the percentage uncertainty in the indicated factor. The 26% over-all systematic uncertainty includes additional contributions from the electron detection efficiency, the radiative corrections to σ_{tot}, and knowledge of the acceptance.

Missing-mass cuts	1.09 (4)
Radiative effects	1.23 (5)
Scanning losses	1.05 (5)
Measuring losses	1.05 (5)
Counter positions and dead time	1.04 (2)
K decay in flight	1.42 (10)
K absorption	1.01 (0)
Ambiguous events	1.04 (0)
Background	0.83 (20)
Dikaon-mass cuts	1.00 (0)
Unseen decay modes	2.04 (2)
Total	3.88 (26)

$$h = \left[\frac{(s - q^2 - m^2)^2 - 4q^2 m^2}{(s - m_\rho^2 - m^2)^2 - 4 m_\rho^2 m^2}\right]^{1/2} . \tag{26}$$

To evaluate Eq. (25) we need three assumptions:

(1) The forward ρ^0 electroproduction cross section comes from the imaginary part of the scattering amplitude. This assumption is supported by lack of strong s dependence in the cross section, the lack of evidence for helicity-nonconserving amplitudes, and the near maximal transverse-longitudinal interference term.

(2) The momentum transfer distributions are the same for transverse and longitudinal ρ^0 production. As we noted in Sec. III B, there is no evidence to the contrary.

(3) The longitudinal $\rho^0 p$ total cross section is less than or equal to the transverse $\rho^0 p$ cross sections as determined by photoproduction of ρ^0 mesons from complex nuclei. VMD models [8] would predict $\sigma_L(\rho^0 p) < \sigma_T(\rho^0 p)$ since they identify

$$(\xi^2)^{1/2} = \frac{\sigma_L(\rho^0 p)}{\sigma_T(\rho^0 p)} , \tag{27}$$

where ξ^2 is determined experimentally by Eq. (19). We take $\sigma_L(\rho^0 p) = \sigma_T(\rho^0 p) = 27.5$ mb.[30]

Using these assumptions and the values in Table III it is straightforward to evaluate $\sigma_L(\gamma^* p)$ from Eq. (25) and correspondingly R_{tot}. At the one-standard-deviation level, the lower bounds for R_{tot} are 0.045, 0.079, and 0.001, corresponding to the $q^2 = -0.36$, -0.70, and -1.27 (GeV/c)^2 bins. These values are plotted in Fig. 15 along with the highest s values $(10.9 \le s \le 16.0$ GeV$^2)$ of R_{tot} determined by Miller *et al.*[27]

As Sakurai has emphasized,[29] these lower bounds on R_{tot} rule out the form

$$R_{tot} = -q^2/\nu^2 \tag{28}$$

in our kinematic region, but are consistent with

$$R_{tot} = \text{constant} = 0.18 . \tag{29}$$

Equation (29) cannot be correct at all q^2, however, since $R_{tot} \to 0$ as $|q^2| \to 0$.

VII. CONCLUSIONS

We have measured the reaction $\gamma^* p \to \rho^0 p$ as a function of the γ^* mass squared q^2 and have observed the following behavior:

(1) The dipion mass spectrum becomes more "normal" as $|q^2|$ increases.

(2) The momentum-transfer distribution broadens as $|q^2|$ increases, indicating a shrinking of the photon in some theoretical treatments.[24]
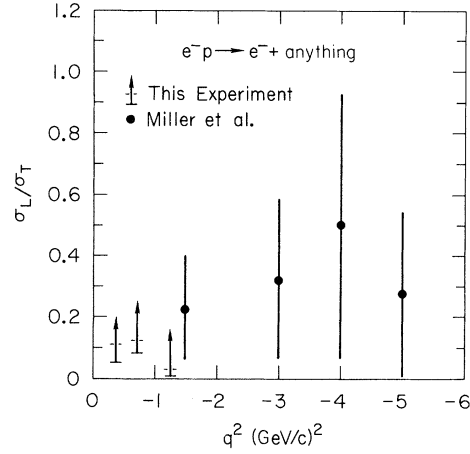
(3) There is no evidence for s-channel helicity

FIG. 15. Lower bounds on R_{tot}, the longitudinal-transverse ratio in inelastic electron scattering, at the one-standard-deviation level. The dashed cross bars indicate the lower bound at the zero-standard-deviation level, or alternatively the lower bound derived from the values in Table III, assuming all experimental errors to be zero. The highest-s-value data from the single-arm experiment (Ref. 27) are also shown.

nonconservation. The production of longitudinally polarized ρ^0 mesons increases with $|q^2|$ at a much larger rate than can be accommodated by a VMD-model interpretation of deep-inelastic electron scattering.[10] The interference between transverse and longitudinal amplitudes is almost maximal.

(4) The cross section decreases with $|q^2|$ roughly as the ρ^0 propagator squared, $(1 - q^2/m_\rho^2)^{-2}$.

We have also observed that the cross section for $\gamma^* p \to \phi p$ decreases with $|q^2|$.

We have calculated lower bounds on the longitudinal-transverse ratio, R_{tot}, and inelastic electron scattering, and have concluded that $R_{tot} \gg -q^2 \nu^{-2}$ in our kinematic region.

[1]J. T. Dakin, G. J. Feldman, W. L. Lakin, F. Martin, M. L. Perl, E. W. Petraske, and W. T. Toner, Phys. Rev. Lett. <u>30</u>, 142 (1973).

[2]D. E. Andrews, K. Berkelman, D. G. Cassel, D. L. Hartill, J. Hartmann, R. Kerchner, E. Lazarus, R. M. Littauer, R. L. Loveless, R. Rohlfs, D. H. White, and A. J. Sadoff, Phys. Rev. Lett. <u>26</u>, 864 (1971).

[3]E. D. Bloom, R. L. A. Cottrell, H. DeStaebler, C. L. Jordan, G. Miller, H. Piel, C. Prescott, R. Siemann, C. K. Sinclair, S. Stein, and R.E. Taylor, Phys. Rev. Lett. <u>28</u>, 516 (1972).

[4]C. Driver, K. Heinloth, K. Hohne, G. Hofmann, F. Janata, P. Karow, D. Schmidt, G. Specht, and J. Rathje, Nucl. Phys. <u>B38</u>, 1 (1972); <u>B53</u>, 643(E) (1973).

[5]V. Eckardt, H. J. Gebauer, P. Joos, H. Meyer, B. Naroska, D Notz, W. J. Podolsky, G. Wolf, S. Yellin, H. Dau, G. Drews, D. Greubel, W. Meincke, H. Nagel, and E. Rabe, Nucl. Phys. <u>B55</u>, 45 (1973).

[6]J. Ballam, E. D. Bloom, J. T. Carroll, G. B. Chadwick, R. L. A. Cottrell, M. Della Negra, H. DeStaebler, L. K. Gershwin, L. P. Keller, M. D. Mestayer, K. C. Moffeit, C. Y. Prescott, and S. Stein, SLAC Report No. SLAC-PUB-1163, 1972 (unpublished).

[7]H. Fraas and D. Schildknecht, Nucl. Phys. <u>B14</u>, 543 (1969).

[8]C. F. Cho and G. J. Gounaris, Phys. Rev. <u>186</u>, 1619 (1969).

[9]G. Kramer and H. R. Quinn, Nucl. Phys. <u>B55</u>, 222 (1973); G. Preparata, Phys. Lett. <u>36B</u>, 53 (1971); M. Sakuraoka, Nuovo Cimento Lett. <u>3</u>, 89 (1972).

[10]J. J. Sakurai and D. Schildknecht, Phys. Lett. <u>40B</u>, 121 (1972); <u>41B</u>, 489 (1972); <u>42B</u>, 216 (1972).

[11]N. Dombey, Rev. Mod. Phys. <u>41</u>, 236 (1969).

[12]L. N. Hand, Phys. Rev. <u>129</u>, 1834 (1963).

[13]F. Martin, S. J. St. Lorant, and W. T. Toner, Nucl. Instrum. Methods <u>103</u>, 503 (1972); A. C. Newton, F. Martin, S. J. St. Lorant, and W. T. Toner, Rev. Sci. Instrum. <u>44</u>, 244 (1973); F. Martin and S. J. St.

Lorant, J. Appl. Phys. <u>44</u>, 460 (1973).

[14]W. L. Lakin, E. W. Petraske, and W. T. Toner, Nucl. Instrum. Methods <u>103</u>, 431 (1972).

[15]W. L. Lakin and R. E. Baggs, Nucl. Instrum. Methods <u>102</u>, 367 (1972).

[16]J. L. Brown, SLAC Report No. SLAC-PUB-752, 1970 (unpublished).

[17]G. Miller, SLAC Report No. SLAC-129, 1971 (unpublished).

[18]A. Bartl and P. Urban, Acta Phys. Austrica <u>24</u>, 139 (1966).

[19]I. Dammann, C. Driver, K. Heinloth, G. Hofmann, F. Janata, P. Karow, D. Luke, D. Schmidt, and G. Specht, Nucl. Phys. <u>B54</u>, 355 (1973).

[20]J. D. Jackson, Nuovo Cimento <u>34</u>, 1645 (1964).

[21]J. Ballam, G. B. Chadwick, Y. Eisenberg, E. Kogan, K. C. Moffeit, P. Seyboth, I. O. Skillicorn, H. Spitzer, G. Wolf, H. H. Bingham, W. B. Fretter, W. J. Podolsky, M. S. Rabin, A. H. Rosenfeld, and G. Smadja, Phys. Rev. D <u>7</u>, 3150 (1973). We use the 9.3-GeV data only.

[22]M. Ross and L. Stodolsky, Phys. Rev. <u>149</u>, 1172 (1966).

[23]F. Bulos, W. Busza, R. Giese, E. Kluge, R. Larsen, D. W. G. S. Leith, and S. H. Williams, in *Proceedings of the Sixteenth International Conference on High Energy Physics, National Accelerator Laboratory, Batavia, Ill., 1972,* edited by J. D. Jackson and A. Roberts (NAL, Batavia, Ill., 1973). We use 9 to 13 GeV data only.

[24]H. T. Nieh, Phys. Lett. <u>38B</u>, 100 (1972); H. Cheng and T. T. Wu, Phys. Rev. <u>183</u>, 1324 (1969); J. D. Bjorken, J. B. Kogut, and D. E. Soper, Phys. Rev. D <u>3</u>, 1382 (1971); J. B. Kogut, *ibid.* <u>5</u>, 1152 (1972).

[25]B. Dieterle, Nuovo Cimento <u>11A</u>, 523 (1972).

[26]K. C. Moffeit (private communication).

[27]G. Miller, E. D. Bloom, G. Buschhorn, D. H. Coward, H. DeStaebler, J. Drees, C. L. Jordan, L. W. Mo, R. E. Taylor, J. I. Friedman, G. C. Hartmann, H. W. Kendall, and R. Verdier, Phys. Rev. D <u>5</u>, 528 (1972).

[28]G. Knies, Phys. Lett. <u>27B</u>, 288 (1968).

[29]J. J. Sakurai, Phys. Rev. Lett. <u>30</u>, 245 (1973). This application was first brought to our attention by J. J. Sakurai in a seminar he gave at SLAC in December 1971.

[30]See K. Gottfried, in *Proceedings of the 1971 International Symposium on Electron and Photon Interactions at High Energies,* edited by N. B. Mistry (Cornell Univ. Press, Ithaca, N.Y., 1972).